

RESEARCH ARTICLE | AUGUST 29 2023

## Sub-GHz resolution line-by-line pulse shaper for driving superconducting circuits

Dahyeon Lee ; Takuma Nakamura ; Andrew J. Metcalf ; Nathan E. Flowers-Jacobs ; Anna E. Fox ; Paul D. Dresselhaus ; Franklyn Quinlan 



APL Photonics 8, 086115 (2023)

<https://doi.org/10.1063/5.0157003>

 CHORUS

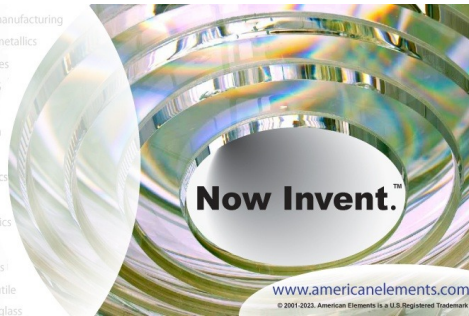


CrossMark



yttrium iron garnet, zeolites, nano ribbons, epitaxial crystal growth, cerium oxide polishing powder, surface functionalized nanoparticles, rare earth metals, osmium, refractory metals, anodic titanium niobate, ZnS, perovskite crystals, spintronics, raman substrates, silver nanoparticles, MOCVD, beta-barium borate, quantum dots, scintillation Ce:YAG, laser crystals, niobate, InAs wafers, MOFs, AuNPs, CdTe, transparent ceramics

glassy carbon, beamsplitters, fused quartz, additive manufacturing, III-IV semiconductors, gallium lump, copper nanoparticles, organometallics, barium fluoride, europium phosphors, photonics, infrared dyes, ultra high purity materials, transparent ceramics, CIGS, cermet, nanodispersions, MBE grade materials, thin film, OLED lighting, solar energy, sputtering targets, fiber optics, h-BN, deposition slugs, CVD precursors, photovoltaics, metamaterials, borosilicate glass, YBCO superconductors, InGaAs, indium tin oxide, MgF2, rutile, diamond micropowder, optical glass



**Now Invent.™**

[www.americanelements.com](http://www.americanelements.com)

© 2001-2022, American Elements LLC, a U.S. Registered Trademark

The Next Generation of Material Science Catalogs

# Sub-GHz resolution line-by-line pulse shaper for driving superconducting circuits

Cite as: APL Photon. 8, 086115 (2023); doi: 10.1063/5.0157003

Submitted: 4 May 2023 • Accepted: 7 August 2023 •

Published Online: 29 August 2023



View Online



Export Citation



CrossMark

Dahyeon Lee,<sup>1,2,a)</sup> Takuma Nakamura,<sup>1,2</sup> Andrew J. Metcalf,<sup>3</sup> Nathan E. Flowers-Jacobs,<sup>4</sup>   
Anna E. Fox,<sup>4</sup> Paul D. Dresselhaus,<sup>4</sup> and Franklyn Quinlan<sup>2,5,b)</sup>

## AFFILIATIONS

<sup>1</sup>Department of Physics, University of Colorado Boulder, Boulder, Colorado 80309, USA

<sup>2</sup>Time and Frequency Division, National Institute of Standards and Technology, Boulder, Colorado 80305, USA

<sup>3</sup>Space Vehicles Directorate, Air Force Research Laboratory, Kirtland AFB, New Mexico 87117, USA

<sup>4</sup>RF Technology Division, National Institute of Standards and Technology, Boulder, Colorado 80305, USA

<sup>5</sup>Electrical, Computer and Energy Engineering, University of Colorado, Boulder, Colorado 80309, USA

<sup>a)</sup>Author to whom correspondence should be addressed: [dahyeon.lee@colorado.edu](mailto:dahyeon.lee@colorado.edu)

<sup>b)</sup>Electronic mail: [fquinlan@nist.gov](mailto:fquinlan@nist.gov)

## ABSTRACT

We demonstrate a sub-GHz resolution, fully programmable Fourier-domain pulse shaper capable of generating arbitrary optical pulse patterns for superconducting circuit platforms. This high resolution allows line-by-line pulse shaping of a 1 GHz-spaced comb, and the pulse shaper can accommodate an optical bandwidth as large as 1 THz, which represents the highest resolution programmable line-by-line pulse shaping to our knowledge. Linear optical sampling with a dual-comb system confirms independent control of 1 GHz-spaced optical lines, and the low phase noise of the pulse shaper is characterized. We apply the pulse shaper as an optical drive for an array of Josephson junctions operating at a temperature of 4 K, where cryogenic photodetection of pulse doublets with user-defined separation characterizes the Josephson junction response. Furthermore, we demonstrate a pulse-density modulation pattern of 4 ps duration optical pulses that can serve as the high bandwidth drive of a quantum-based Josephson arbitrary waveform synthesizer. By leveraging the exquisite control, large bandwidth, and low noise of photonics, this represents an important advance toward the realization of high power and high spectral purity AC voltage standards at gigahertz frequencies without requiring 100 GHz bandwidth driving electronics.

© 2023 Author(s). All article content, except where otherwise noted, is licensed under a Creative Commons Attribution (CC BY) license (<http://creativecommons.org/licenses/by/4.0/>). <https://doi.org/10.1063/5.0157003>

## I. INTRODUCTION

Microwave photonics,<sup>1</sup> where optical systems are employed to transport, filter, generate, or otherwise process microwave and millimeter wave signals, has found application in diverse fields such as telecommunications,<sup>2</sup> radar,<sup>3</sup> and radio astronomy.<sup>4</sup> Microwave photonic systems take advantage of the large bandwidth, low loss, and low noise of optical systems, as well as the long reach of optical fiber interconnects. Recently, there has been renewed interest in exploiting photonic links to connect room temperature microwave sources to superconducting circuits, motivated by the unique challenges inherent in transporting microwave and millimeter-wave

signals into a cryogenic environment.<sup>5–8</sup> For example, wiring up a large number of coaxial cables can present a significant heat load in quantum information processing systems that rely on superconducting qubits,<sup>9</sup> whereas the thermal conductivity of optical fiber is ~1000 times less. Moreover, the materials and cable lengths used to reduce the heat load of coaxial cabling also tend to be lossy at high frequencies. This limits the ability to transmit high bandwidth signals, directly impacting applications such as superconducting computing.<sup>10,11</sup> In contrast, optical sources can readily generate >1 THz of bandwidth, and optical fibers can transport RF, microwave, and mm-wave signals with negligible signal distortion and loss. When combined with high-speed photodiodes compatible

with cryogenic operation,<sup>5,7,12,13</sup> cryogenic photonic links become an attractive solution for delivering signals to superconducting platforms.

An application that can greatly benefit from cryogenic photonic links is the Josephson arbitrary waveform synthesizer (JAWS),<sup>14</sup> summarized in Fig. 1. JAWS is an instrument for producing quantum-based AC voltage standards with an amplitude traceable to fundamental constants and a precision error of less than one part in  $10^7$ .<sup>15</sup> Such low uncertainty is achieved by exploiting the fact that when a superconducting (temperature  $\sim 4$  K) Josephson junction is driven with a current pulse, it emits a quantized voltage pulse with a time-integrated area of exactly  $nh/(2e)$ , where  $n$  is an integer,  $h$  is the Planck constant, and  $e$  is the elementary charge. The JAWS architecture relies on a current pulse pattern that encodes the target waveform with pulse density modulation using a delta-sigma algorithm.<sup>16</sup> This produces a pattern of quantized voltage pulses that are then low-pass filtered to produce the desired voltage waveform. Importantly, the bandwidth of the driving pulse pattern should be roughly 100 times higher than the target synthesis frequency. While high precision has been demonstrated at audio frequencies near 1 kHz, applications such as developing quantum-based calibration

standards for 5G wireless communication and quantum information systems require a million-fold increase in the frequency to gigahertz frequencies or higher.<sup>17,18</sup> Therefore, scaling JAWS to these higher frequencies will require a driving pulse pattern bandwidth greater than 100 GHz.

The driving bandwidth requirements of gigahertz-rate JAWS are difficult to achieve with standard electronics since no commercial RF arbitrary pulse pattern generator with such a high bandwidth is available, and maintaining the high bandwidth with low distortion over a coaxial cable is challenging. As a result, alternative means to synthesize quantum-accurate gigahertz waveforms have been investigated, such as approaches based on single-flux-quantum pulses and cryogenic memory.<sup>19</sup> Here we investigate a microwave photonics approach to generate user-defined, complex, and high bandwidth waveforms with high fidelity. The driving pulse pattern is generated optically, routed into the cryostat via optical fiber, and converted to a current pulse pattern with a photodiode placed near the Josephson junction array. Our approach takes direct advantage of the bandwidth native to optical systems and has the potential to utilize the low noise inherent in optical clocks and oscillators.

A key element of the cryogenic photonic link is an optical arbitrary pulse pattern generator. In the context of driving superconducting circuits, several avenues have been pursued to optically generate pulse patterns, including the multi-stage pulse interleaving method of Ref. 20, the pulse picking technique of Ref. 21, and the optical time domain multiplexing (OTDM) approach of Ref. 22. However, these methods either cannot generate arbitrary pulse patterns, cannot generate high-bandwidth pulse patterns, or require the added cost and complexity of multiple high-speed electronics to drive fast electro-optic modulators. We instead opt for a frequency domain solution for generating arbitrary pulse patterns based on Fourier-domain pulse shaping of an optical frequency comb.<sup>23–25</sup> By operating on the comb's discrete frequency components, we produce arbitrary pulse patterns that are periodic with the input pulse rate without the need for any high-speed electronics. Our high-resolution pulse shaper is capable of line-by-line pulse shaping on frequency combs with 1 GHz spacing, demonstrating fully programmable gray-level amplitude and phase controls and a  $>30$  dB extinction ratio. The pulse shaper can accommodate 1 THz of optical bandwidth, corresponding to a time-bandwidth product greater than 1000. While previous study has shown pulse shaping on an 890 MHz comb,<sup>26</sup> fully independent, gray-level, programmable control of the comb lines has not yet been demonstrated with  $\sim 1$  GHz resolution. Our work represents the highest resolution programmable pulse shaping demonstrated to date for Fourier-domain pulse shapers of which we are aware.

In Sec. II, we describe the setup and characterization of the pulse shaper, including dual-comb measurements of the shaper's capabilities and phase noise measurements. Section III reports on pulse pattern generation, including a complex waveform geared toward driving Josephson junction arrays. We then demonstrate the direct application of the pulse shaper to a superconducting platform, described in Sec. IV, by driving an array of 1500 Josephson junctions with pulse doublets, producing Shapiro voltage steps whose size is dependent on the driving pulse separation. In Section V, we conclude.

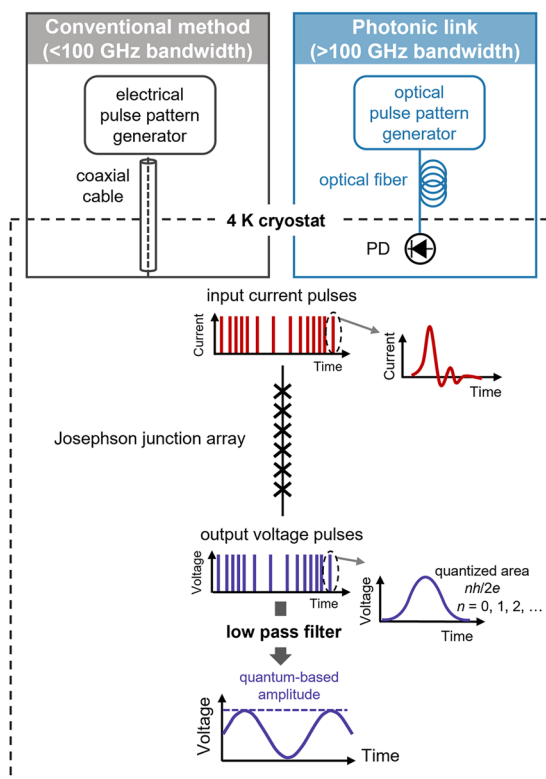


**FIG. 1.** Concept of optically driven Josephson arbitrary waveform generator. An array of Josephson junctions is driven with current pulses from a photodiode. The voltage pulses produced by the Josephson junctions have a quantized area and provide traceability to fundamental constants. The target waveform is encoded with pulse density modulation. Photonic links can provide much higher bandwidths than conventional methods based on electronic pulse pattern generators and coaxial cables.  $h$ : Planck constant;  $e$ : elementary charge.

## II. PULSE SHAPER CHARACTERIZATION

Our target application of driving Josephson junction arrays imposes demanding requirements on the pulse shaper, especially on its resolution. As our aim is to synthesize frequencies for JAWS between 1 and 2 GHz, we correspondingly designed our shaper with the capability to generate a pulse-density modulated pattern that repeats at a rate of 1–2 GHz. This in turn corresponds to 1–2 GHz repetition rate for the input comb. In addition, the generated pulse pattern should fill the entire time window, i.e., the pulses can be placed anywhere within the pulse repetition period, requiring line-by-line pulse shaping.<sup>23,27</sup> Line-by-line pulse shaping on frequency combs with 1–2 GHz line spacing is quite challenging due to the high resolution necessary to resolve the comb lines. In fact, to resolve 1 GHz comb lines with a diffraction grating with a line density of 1740 lines/mm (close to the highest useable line density at our 1064 nm operating wavelength), the diffraction grating would need to be larger than 15 cm. Importantly, a Rayleigh-like resolution criterion for the comb lines is not sufficient for line-by-line pulse shaping because this would induce significant crosstalk between adjacent lines. In practice, a 2–3 times higher resolving power would be more desirable, and the required size for the diffraction grating would be proportionally larger. We instead use a 2D pulse shaper that employs two spectral dispersers,<sup>26,28,29</sup> in which a virtually imaged phased array (VIPA) is used in conjunction with a conventional grating.<sup>30</sup> Taking advantage of the very high resolution of the VIPA and the broad bandwidth of the diffraction grating, we achieve line-by-line pulse shaping on 1–2 GHz combs.

A schematic diagram of the pulse shaper is shown in Fig. 2(a). The input light source was an electro-optic (EO) comb consisting of three phase modulators and one intensity modulator, whose

repetition rate was switched between 1 and 2 GHz, depending on the particular characterization measurement or waveform we wished to investigate. The number of comb lines was  $\sim 150$ . The central wavelength of 1064 nm was chosen instead of the more conventional 1550 nm in order to accommodate the cryogenic operation of InGaAs photodiodes. Due to the bandgap shift with temperature, standard InGaAs photodiodes do not respond to 1550 nm light when cooled to cryogenic temperatures.<sup>31</sup> The comb light was routed to a fiberized circulator and then launched into free space. A cylindrical lens focused the beam in a line to match the entrance slit of the VIPA. The VIPA free spectral range (FSR) is 30.3 GHz with a manufacturer-specified finesse of 85, corresponding to a full width at half maximum (FWHM) resolution of 360 MHz. Although the VIPA exhibits very high spectral resolution, it has the disadvantage that frequencies separated by the VIPA FSR are dispersed at the same angle. A second spectral disperser, a transmission volume holographic grating in our case, is commonly used to further separate comb lines in the orthogonal spatial dimension,<sup>26,28,29,32–34</sup> resulting in a “frequency brush” pattern shown in Fig. 2(b). After the comb lines were spatially separated, they were focused onto a  $1920 \times 1200$  2D spatial light modulator (SLM) with two cylindrical lenses. The phase and amplitude of  $\sim 300$  optical spots were controlled by the SLM ( $\sim 150$  comb lines  $\times 2$  VIPA diffraction orders). The size of the SLM can accommodate 1 THz of bandwidth, although we only utilized  $\sim 300$  GHz in our experiments. The reflected light retraced its path to form the pulse shaper output at the circulator. The overall insertion loss of the pulse shaper, measured from the circulator input to the circulator output, was  $\sim 15$  dB, comparable to that of other 2D pulse shapers.<sup>26,28</sup> The pulse shaper was aligned for zero temporal dispersion by monitoring spectral ripples at the VIPA FSR.<sup>35</sup>

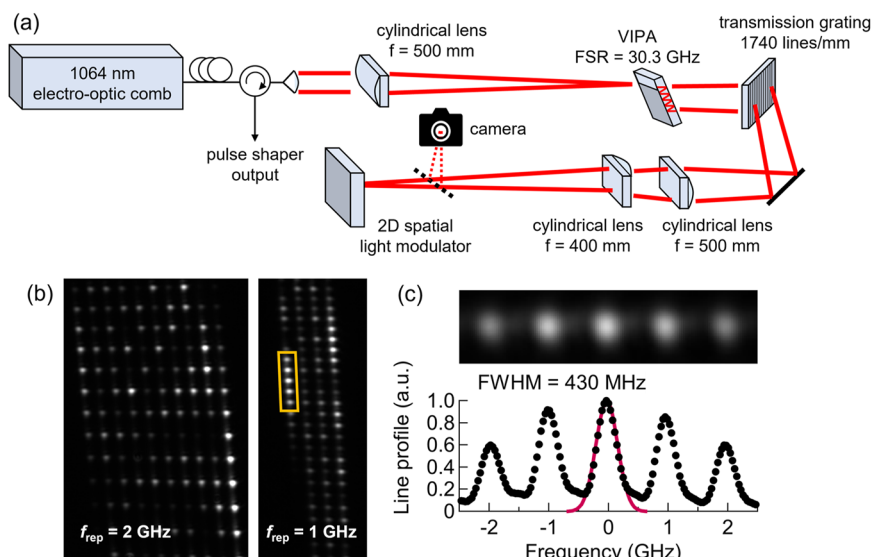


**FIG. 2.** (a) 2D VIPA-based pulse shaper setup. The input comb modes are spatially dispersed in a 2D pattern. The dispersion pattern is imaged with a camera when the light is diverted away from the spatial light modulator with a removable mirror (dotted lines). (b) Camera images of the 2D dispersion pattern for 2 and 1 GHz combs. The comb modes are clearly resolved. (c) Line profile of the highlighted section in (b). A Gaussian fit yields 430 MHz FWHM resolution (red). VIPA: virtually imaged phased array; FWHM: full width at half maximum.

The phase and amplitude of individual comb lines were controlled using the method of Ref. 36. A patch of  $15 \times 15$  pixels on the SLM was grouped together, forming a “superpixel.” Simultaneous amplitude and phase control were achieved despite the fact that our SLM is a phase-only device. By applying a sawtooth phase pattern with a period of five pixels to each superpixel, the light incident on the superpixel was diffracted to multiple orders (mostly to the first order for full  $2\pi$ -depth phase modulation). The first order diffraction was used as the output of the pulse shaper, and the strength of this diffraction order was controlled by changing the depth of phase modulation, i.e., the sawtooth amplitude. We used the first order diffraction as the output to mitigate the effect of the dead space between the SLM pixels (95% fill factor), which was crucial for achieving a  $>30$  dB extinction ratio. This comes at the cost of a slightly higher loss compared to using the zeroth order.<sup>28</sup> For coarse phase control in steps of  $0.4\pi$  ( $2\pi$ /sawtooth period), the sawtooth grating was spatially translated by one pixel.<sup>37</sup> Fine phase control was added by applying an additional phase to the entire superpixel.

The high resolution of the pulse shaper was verified by the camera images shown in Figs. 2(b) and 2(c). In order to image the dispersion pattern at the plane of the SLM, the light was temporarily routed to a camera with a removable mirror, essentially forming a VIPA-based spectrometer. Even for 1 GHz comb line spacing, individual comb lines are clearly resolved. Figure 2(c) (top) is a zoomed-in view of the highlighted region in Fig. 2(b). A Gaussian fit to its line profile yields 430 MHz FWHM resolution, close to the 360 MHz resolution estimated earlier [Fig. 2(c), bottom]. The asymmetry in the line shape has been observed in other VIPA-based pulse shapers and spectrometers.<sup>26,38,39</sup> The camera images also played a crucial role in the pulse shaper’s wavelength-to-pixel mapping (see the supplementary material for more details).

We characterized the resolution of our pulse shaper using a dual-comb measurement.<sup>40–42</sup> Dual-comb measurements can provide magnitude and phase information imprinted on individual comb lines via multiheterodyne detection with a second comb. The response of the pulse shaper could thus be characterized on a line-by-line basis without the need for a sub-GHz resolution spectrometer. By showing that the pulse shaper can independently manipulate the modes of a 1 GHz comb, we infer that the pulse shaper has a sub-GHz resolution. The measurement setup is shown schematically in Fig. 3(a). A 1064 nm diode laser was used as the seed for two EO combs with repetition rates of 1 GHz and 999.5 MHz ( $\Delta f_{\text{rep}}$  of 500 kHz). The two combs were generated from two phase-correlated channels of a single RF synthesizer. Using a common seed laser and synthesizer made our measurement considerably simpler because there was no need for multiple phase locks that force coherence between the two combs. A 100 MHz acousto-optic modulator was installed in one branch so that the resulting RF comb would be centered at 100 MHz. After the comb passed through the pulse shaper, it was combined with the second comb and illuminated a photodiode. The time-domain interferogram was digitized, and Fourier transformation was performed to extract the phase and amplitude of the multiheterodyne RF comb lines. For data acquisition, a 20  $\mu\text{s}$  time window containing ten periods of the interferogram was sampled at 500 MHz with an oscilloscope, and 64 averages were performed.

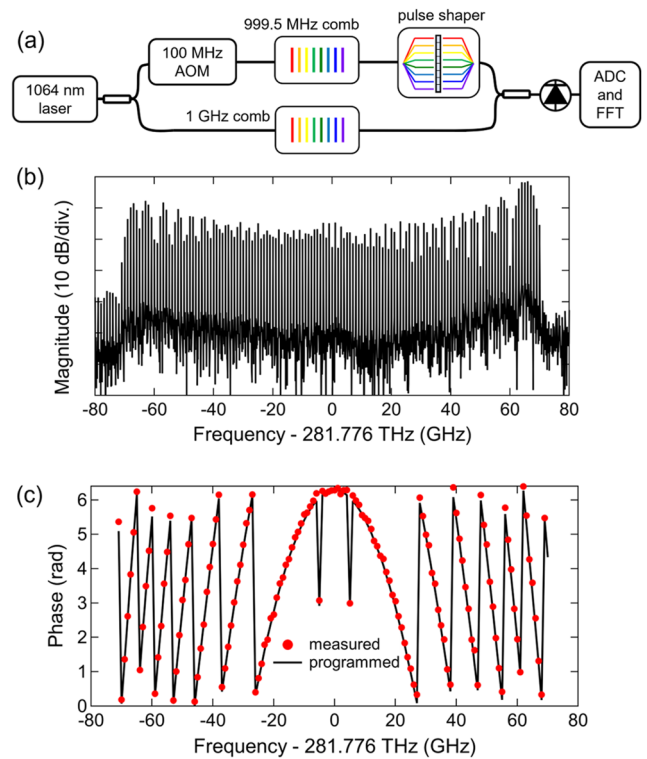


**FIG. 3.** (a) Dual-comb measurement setup for characterizing the resolution of the pulse shaper. (b) Power spectrum of the dual-comb signal, showing the  $\sim 150$  comb lines controlled by the pulse shaper. (c) Comparison between the spectral phase programmed into the pulse shaper and the measured phase. There are two places near the middle where  $\pi$  phase shifts were intentionally programmed. An abrupt  $\pi$  phase shift between adjacent lines shows that the pulse shaper is operating in the line-by-line regime even for 1 GHz spacing. AOM: acousto-optic modulator; ADC: analog-to-digital converter; FFT: fast Fourier transform.

The magnitude and phase information retrieved from the dual-comb measurement are shown in Figs. 3(b) and 3(c). The magnitude spectrum of Fig. 3(b) shows the  $\sim 150$  comb lines controlled by the pulse shaper. Since the pulse shaper was programmed to apply a phase-only mask, the magnitude spectrum shown here is simply the product of the spectra of the two combs up to a scaling factor. No effort was taken to optimize the combs for spectral flatness. Figure 3(c) shows the spectral phase applied by the pulse shaper. To measure the phase response, a reference measurement was first taken with no phase mask programmed on the pulse shaper. Then, the pulse shaper was programmed to apply a phase mask shown as the black line. The red dots are the spectral phase differences between the second and first measurements for each comb line. The match between the measured and programmed phases is excellent. However, a more interesting feature is that there are two places near the middle where abrupt  $\pi$  phase shifts were intentionally applied. The ability to apply such a large phase shift between adjacent lines is a hallmark of line-by-line pulse shaping and shows that the crosstalk between adjacent lines is not significant.<sup>43</sup> The ability to perform line-by-line pulse shaping on a 1 GHz comb shows that the pulse shaper has a sub-GHz resolution. With sub-GHz resolution and

1 THz bandwidth, our pulse shaper should be able to generate complex waveforms with time-bandwidth products exceeding 1000 if the full bandwidth is utilized.

We also characterized the phase noise added by the pulse shaper. The timing jitter of the synthesized waveform from JAWS should inherit the timing jitter of the driving pulse repetition rate, provided that the pulse shaper does not add excessive noise. We measured the phase noise of the 2 GHz repetition rate of the comb after it transited through the pulse shaper. The phase noise measurement setup is shown in Fig. 4(a). The 2 GHz comb output was split into two branches and amplified with ytterbium-doped fiber amplifiers (YDFA). One of the branches contained the pulse shaper that was programmed to apply flat amplitude and phase masks. To confirm the measurement floor, a separate phase noise measurement was taken with the pulse shaper bypassed. The 2 GHz repetition rate was photodetected and bandpass filtered, and the relative phase of the two 2 GHz signals was compared at the mixer. Figure 4(b) shows the measured phase noise of the pulse shaper on the 2 GHz repetition rate (black trace). At offset frequencies below 1 kHz, the phase noise of the pulse shaper is comparable to that of a commercial synthesizer, shown in green. The phase noise between 100 Hz and 1 kHz is mainly due to the long air path within the pulse shaper, which was confirmed by shutting off the SLM such that no active element was present in the pulse shaper. In terms of frequency stability, this level of phase noise corresponds to a fractional frequency instability below  $1 \times 10^{-13}$  at 1 s, which is better than most RF frequency references such as quartz oscillators and H-masers. The

lower white noise floor of the black trace is due to a lower level of amplified spontaneous emission (ASE) from the YDFA incident on the photodiode—since the pulse shaper is centered at 1064 nm, it rejects the ASE peak at 1030 nm even when it is programmed to transmit everything. Therefore, it acts as an excellent ASE rejection filter, lowering the white measurement floor. The remaining white floor is dominated by the ASE at the signal wavelength of 1064 nm and may be improved by increasing the optical power seeding the amplifier beyond the  $\sim 50 \mu\text{W}$  used here.

### III. PULSE PATTERN GENERATION

Creating a typical pulse pattern for a JAWS based on a delta-sigma algorithm requires defining a clock rate for the pulses, that is, a maximum pulse repetition rate, and a length for the pulse pattern. In general, it is advantageous for the clock rate to be as fast as possible and for the pattern length to be as long as possible. It is, therefore, necessary to compress the pulses as much as possible, preferably to their transform limit, demonstrate variable pulse delays, and, finally, demonstrate arbitrary, user-defined pulse pattern generation. In this work, we are aiming to demonstrate a JAWS pulse pattern with a 100 GHz clock rate and a pattern length of 50 clock steps, which would generate a 2 GHz tone.

With the pulse shaper, we compressed the output of a 2 GHz EO comb to near the transform limit. The output of the EO comb was a quasi-square wave carved out by the intensity modulator, as shown in Fig. 5(a). For measuring the intensity profile of the pulses, intensity cross correlation with short (500 fs autocorrelation FWHM) reference pulses was used. When the pulse shaper was programmed to apply second and fourth order dispersions of  $137 \text{ ps}^2$  and  $150 \text{ ps}^4$ , respectively, the resulting pulse shape was very close to the calculated transform limit, as shown in Fig. 5(b). No third order dispersion compensation was needed. The discrepancy in the cross correlation trace at one of the wings was confirmed to be due to satellite pulses in the reference pulse train.

While pulse compression requires phase programming only, producing an arbitrary pulse pattern requires amplitude programming as well. As a simple demonstration of amplitude programmability, we generated pulse doublets with arbitrary delays. Pulse doublets are also of practical value because they can be used as a test signal to measure the response speed of the Josephson junctions,<sup>22</sup> discussed in greater detail in Sec. IV. Figure 5(c) shows the generated pulse doublets with arbitrary delays. Although not shown in this figure, any delay within the 500 ps period could be produced. Figure 5(d) shows the measured power of each comb line when the pulse shaper was programmed to produce pulse doublets separated by 30 ps. Ripples at 33 GHz are apparent, as one would expect from the spectral interference of two pulses separated by 30 ps. Gray-level amplitude control was crucial for carving this spectral interference pattern out of the comb spectrum. The expected power, shown in light blue, was calculated by multiplying the pulse shaper output spectrum when nothing was programmed to the pulse shaper with the applied amplitude mask. See the supplementary material for more details on this measurement.

We also generated a pulse pattern suitable for driving a Josephson junction array for synthesizing a 2 GHz sine wave. The pulse pattern is clocked at 100 GHz with a 500 ps repetition period

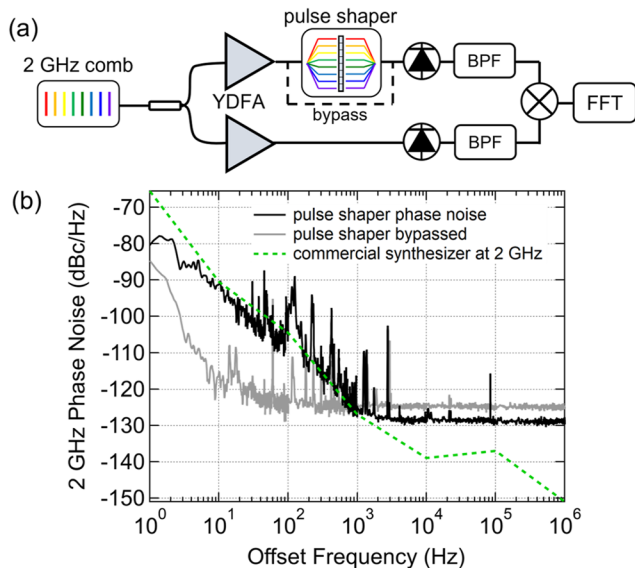


**FIG. 4.** (a) Phase noise measurement setup for the pulse shaper. The excess phase noise of the pulse shaper at the 2 GHz repetition rate was measured. The same measurement was repeated with the pulse shaper bypassed for comparison (dotted line). (b) The phase noise of the pulse shaper is comparable to that of a commercial synthesizer. The white floor is lower when the pulse shaper is included because the pulse shaper rejects the amplified spontaneous emission from the YDFA. YDFA: ytterbium-doped fiber amplifier; BPF: 2 GHz bandpass filter; FFT: fast Fourier transform.

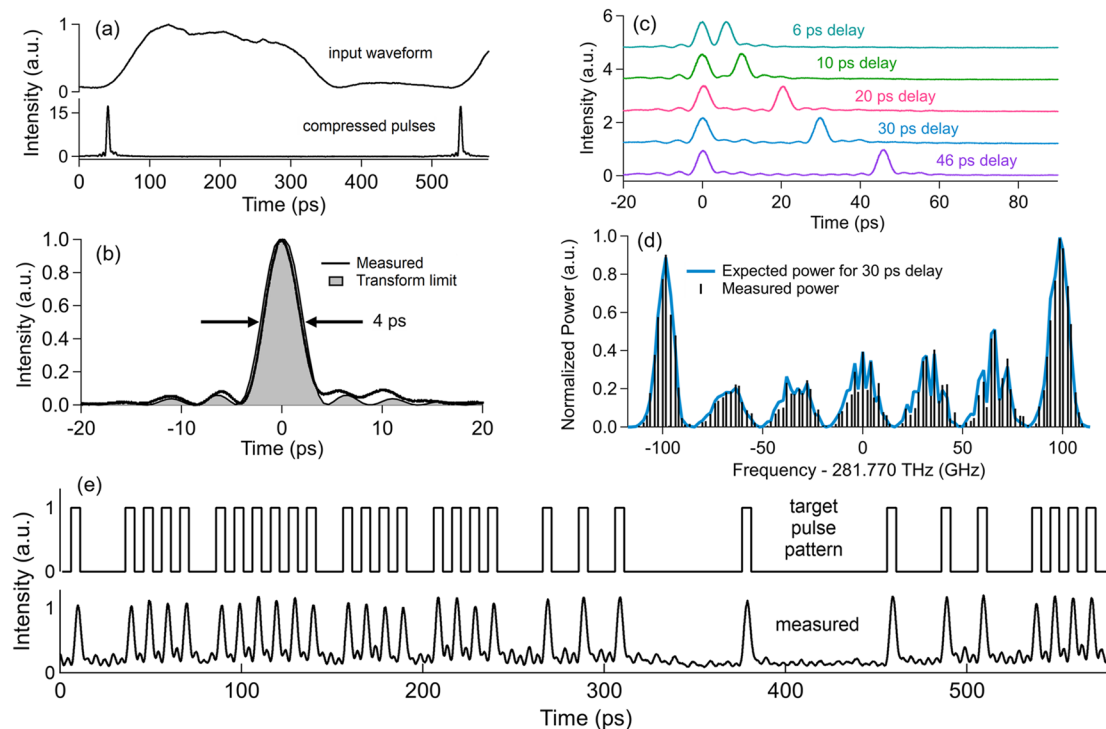


**FIG. 5.** Waveform generation with the pulse shaper. (a) Demonstration of pulse compression, measured with optical intensity cross correlation. The input to the pulse shaper was a quasi-square wave pulse train from an uncompressed electro-optic comb. With the pulse shaper, the square pulses were compressed to near the transform limit. (b) Zoomed in view of the compressed pulses. The discrepancy from the transform limit at one of the wings is due to satellite pulses in the cross correlation reference pulses. (c) Pulse doublets with arbitrary delays. (d) Power of the 2 GHz comb lines when the pulse shaper was programmed to generate pulse doublets with a 30 ps delay. Gray level amplitude control of the pulse shaper enables imparting a 33 GHz modulation onto the spectrum as needed for generating 30 ps doublets. (e) Demonstration of arbitrary pulse pattern generation. This pulse pattern has a period of 50 clock steps at a clock rate of 100 GHz. It uses 25 pulses to generate a 2 GHz sine wave with a dc offset.

(50 clock steps). The number and location of the pulses are chosen using a delta-sigma algorithm to create a 2 GHz waveform with a large amplitude, which results in a pattern with 25 pulses. Figure 5(e) shows a pulse pattern encoding the 2 GHz target waveform and the generated pulse pattern produced by the pulse shaper. The pulse shaper was able to produce this arbitrary pulse pattern without noticeable timing errors. This optical pulse pattern was synthesized with a >200 GHz optical bandwidth, which far exceeds the bandwidth of commercial pulse pattern generators. The final bandwidth of the driving pulse pattern will only be limited by the speed of the photodiode used as an optical-to-electrical converter. The pulse height imbalances and the ripples between the pulses are due to interference between nearby pulses. These imperfections can be tolerated to some degree due to the quantized nature of the voltage pulses produced by the Josephson junctions.<sup>5</sup> We nevertheless attempted to minimize these by manually adjusting the pulse heights and the carrier envelope phases of each pulse with the process outlined in the supplementary material. If needed, iterative feedback control on the synthesized pulse pattern could significantly reduce the pulse height imbalances and ripples.<sup>44–47</sup> Note also that the pulse pattern fills the entire 500 ps period, another hallmark of line-by-line pulse shaping.

#### IV. INTERFACING THE PULSE SHAPER WITH A JOSEPHSON JUNCTION ARRAY

While we have shown that our pulse shaper can generate arbitrary optical pulse patterns for JAWS, important tasks remain before the pulse shaper can fully enable a GHz-JAWS system. First, the optical pulse pattern has to be converted to an electrical pulse pattern with a high-speed (>100 GHz bandwidth) photodiode at 4 K. Second, a Josephson junction array with a correspondingly fast response speed has to be designed. Both challenges are imminently feasible—photodiodes with a bandwidth greater than 300 GHz have been demonstrated,<sup>48</sup> and the response speed of a Josephson junction array can be tuned by adjusting its circuit parameters.<sup>49</sup> Efforts are currently underway to address these challenges.

As part of such efforts, we tested the response of a Josephson junction array to simple pulse patterns generated by the pulse shaper, shown schematically in Fig. 6(a). With line-by-line pulse shaping of a 1 GHz comb, we encoded the pulse shaper to produce short pulses at a 1 GHz repetition rate, pulse doublets with delays of 50, 100, and 500 ps (which essentially doubles the repetition rate to 2 GHz), as well as 3 GHz pulses. The pulse patterns

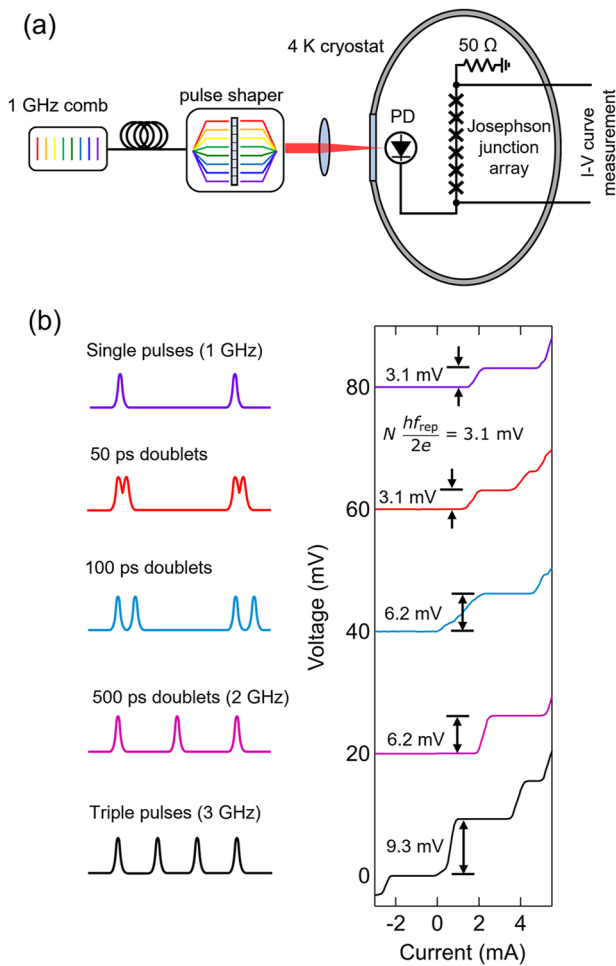


**FIG. 6.** Driving a Josephson junction array with the pulse shaper. (a) Schematic diagram of the experimental setup. (b) I–V curves of a Josephson junction array consisting of 1500 junctions for various input drive pulse patterns. The flat voltage regions can be used for synthesizing voltage waveforms with quantum-based accuracy. Each trace is offset by 20 mV for clarity.  $N$ : number of Josephson junctions in the array;  $h$ : Planck constant;  $f_{\text{rep}}$ : pulse repetition rate;  $e$ : fundamental charge.

were sent into a 4 K cryostat through a window and illuminated a high-speed photodiode. We used a modified uni-traveling carrier photodiode optimized for the 1064 nm wavelength.<sup>50</sup> The FWHM of the current pulses produced by the photodiode was measured at room temperature to be  $\sim 30$  ps, limited by the impulse response of the photodiode. The peak current of the pulses was  $\sim 30$  mA. The output of the photodiode was connected to a chip containing an array of 1500 Josephson junctions with an expected response speed of 100 ps,<sup>51</sup> and the current-voltage (I–V) curve of the Josephson junction array was measured with a four-wire setup via two sets of twisted pair DC lines.

The response of the Josephson junctions to various pulse patterns is shown in Fig. 6(b). When the Josephson junctions were driven with 1 GHz pulses, their I–V curve showed a flat voltage

region that forms the basis of the Josephson voltage standard, called a Shapiro step.<sup>52</sup> The height of the Shapiro step was calculated to be 3.10 mV using the formula  $Nf_{\text{rep}}h/(2e)$ , where  $N = 1500$  is the number of the Josephson junctions,  $f_{\text{rep}}$  is the number of pulses that the Josephson junctions respond to per second, and  $e$  and  $h$  are fundamental constants, and the calculated value agreed with the measured step height of 3.12 mV within the specified uncertainty of our measurement instrument. No attempt was made to achieve metrological accuracy in this demonstration. If the driving pulses are closely spaced compared to the response speed of the junctions, the Josephson junctions cannot distinguish the two pulses, and their I–V curve is qualitatively the same as that for the single pulse drive case. Such behavior can be seen in the I–V curve for the 50 ps doublet drive shown in red, where the size of the Shapiro step remains 3.1 mV. As the pulse spacing becomes larger, the Josephson junctions start to distinguish the two pulses, and the size of the Shapiro step doubles, as can be seen in the light blue and magenta traces. Similarly, the Shapiro step size tripled when the Josephson junctions were driven with a 3 GHz pulse train. These simple demonstrations show that Josephson junctions respond as expected to optical drive, as well as the agility with which the pulse shaper can manipulate the drive pulse pattern.

## V. CONCLUSION

We have demonstrated a 2D VIPA-based pulse shaper with sub-GHz resolution built to optically drive Josephson junction arrays with arbitrary pulse patterns. The high resolution of the pulse shaper enabled line-by-line pulse shaping of a 1 GHz-spaced comb, which is the highest resolution programmable line-by-line pulse shaping reported so far to the best of our knowledge. The phase noise of the pulse shaper was measured to be low enough for use in conjunction with standard microwave sources without degrading the timing stability. Furthermore, we produced pulse doublets with arbitrary delays and used these pulses to characterize the response of an array of 1500 Josephson junctions. With line-by-line pulse shaping of a 2 GHz comb, we compressed the output pulses to near the transform limit and generated a complex pulse pattern consisting of 25 pulses per period with a bandwidth that far exceeds the capabilities of commercial pulse pattern generators. Given that a fast photodiode is used as an optical-to-electrical converter,<sup>53</sup> this work charts a path toward optically driving a Josephson junction array to produce quantum-traceable JAWS waveforms at gigahertz rates without the need for  $>100$  GHz bandwidth driving electronics. More generally, this work demonstrates the advantages brought by microwave photonics, in terms of high bandwidth, low loss, low noise, and signal complexity, to drive superconducting circuit platforms.

## SUPPLEMENTARY MATERIAL

The online version contains supplementary material, including information about the wavelength-to-pixel mapping of the pulse shaper, calculating amplitude and phase masks, 2 GHz line-by-line power measurement with an optical spectrum analyzer, and more details on the Josephson junction optical drive demonstration.

## ACKNOWLEDGMENTS

This work was funded by NIST. We acknowledge J. C. Campbell for supplying the MUTC photodiode and J. A. Brevik for their early contributions to this work. S. A. Diddams and J. D. Teufel provided valuable comments and insights. We further acknowledge K. F. Chang and M. Castellanos-Beltran for their comments on the manuscript.

The views expressed are those of the authors and do not necessarily reflect the official policy or position of the Department of the Air Force, the Department of Defense, or the U.S. government.

## AUTHOR DECLARATIONS

### Conflict of Interest

The authors have no conflicts to disclose.

### Author Contributions

**Dahyeon Lee:** Conceptualization (equal); Formal analysis (lead); Investigation (lead); Writing – original draft (lead); Writing – review & editing (equal). **Takuma Nakamura:** Conceptualization (supporting); Formal analysis (supporting); Investigation (supporting); Writing – review & editing (equal). **Andrew J. Metcalf:** Conceptualization (supporting); Writing – review & editing (equal). **Nathan E. Flowers-Jacobs:** Conceptualization (supporting); Investigation (supporting); Resources (equal); Writing – review & editing (equal). **Anna E. Fox:** Resources (equal). **Paul D. Dresselhaus:** Conceptualization (supporting); Funding acquisition (supporting); Resources (equal); Supervision (supporting). **Franklyn Quinlan:** Conceptualization (equal); Funding acquisition (lead); Investigation (equal); Project administration (lead); Supervision (lead); Writing – original draft (equal); Writing – review & editing (equal).

## DATA AVAILABILITY

The data that support the findings of this study are available from the corresponding author upon reasonable request.

## REFERENCES

- J. Capmany and D. Novak, "Microwave photonics combines two worlds," *Nat. Photonics* **1**, 319–330 (2007).
- C. Lim, A. Nirmalathas, M. Bakaul, P. Gamage, K.-L. Lee, Y. Yang, D. Novak, and R. Waterhouse, "Fiber-wireless networks and subsystem technologies," *J. Lightwave Technol.* **28**, 390–405 (2010).
- P. Ghelfi, F. Laghezza, F. Scotti, G. Serafino, A. Capria, S. Pinna, D. Onori, C. Porzi, M. Scaffardi, A. Malacarne, V. Vercesi, E. Lazzeri, F. Berizzi, and A. Bogoni, "A fully photonics-based coherent radar system," *Nature* **507**, 341–345 (2014).
- J.-F. Cliche and B. Shillue, "Applications of control precision timing control for radioastronomy maintaining femtosecond synchronization in the Atacama large millimeter array," *IEEE Control Syst. Mag.* **26**, 19–26 (2006).
- J. A. Brevik, D. Lee, A. E. Fox, Y. Peng, A. A. Babenko, J. C. Campbell, P. D. Dresselhaus, F. Quinlan, and S. P. Benz, "Bipolar waveform synthesis with an optically driven Josephson arbitrary waveform synthesizer," *IEEE Trans. Appl. Supercond.* **32**, 1–8 (2022).

- O. Kieler, B. Karlsen, P. A. Ohlckers, E. Bardalen, M. N. Akram, R. Behr, J. Ireland, J. Williams, H. Malmbeek, L. Palafox, and R. Wendisch, "Optical pulse-drive for the pulse-driven AC Josephson voltage standard," *IEEE Trans. Appl. Supercond.* **29**, 1–5 (2019).
- F. Lecocq, F. Quinlan, K. Cicak, J. Aumentado, S. A. Diddams, and J. D. Teufel, "Control and readout of a superconducting qubit using a photonic link," *Nature* **591**, 575–579 (2021).
- C. Urano, M. Maruyama, N.-h. Kaneko, H. Yamamori, A. Shoji, M. Maezawa, Y. Hashimoto, H. Suzuki, S. Nagasawa, T. Satoh, M. Hidaka, and S. Kiryu, "Operation of a Josephson arbitrary waveform synthesizer with optical data input," *Supercond. Sci. Technol.* **22**, 114012 (2009).
- S. Krinner, S. Storz, P. Kurpiers, P. Magnard, J. Heinsoo, R. Keller, J. Lütolf, C. Eichler, and A. Wallraff, "Engineering cryogenic setups for 100-qubit scale superconducting circuit systems," *EPJ Quantum Technol.* **6**, 2 (2019).
- M. A. Manheimer, "Cryogenic computing complexity program: Phase 1 introduction," *IEEE Trans. Appl. Supercond.* **25**, 1–4 (2015).
- B. Yin, H. Gevorgyan, D. Onural, A. Khilo, M. A. Popović, and V. M. Stojanović, "Electronic-photon cryogenic egress link," in *ESSCIRC 2021 - IEEE 47th European Solid State Circuits Conference (ESSCIRC)* (IEEE, 2021), pp. 51–54.
- E. Bardalen, B. Karlsen, H. Malmbeek, O. Kieler, M. N. Akram, and P. Ohlckers, "Packaging and demonstration of optical-fiber-coupled photodiode array for operation at 4 K," *IEEE Trans. Compon., Packag., Manuf. Technol.* **7**, 1395–1401 (2017).
- E. Bardalen, B. Karlsen, H. Malmbeek, M. N. Akram, and P. Ohlckers, "Evaluation of InGaAs/InP photodiode for high-speed operation at 4 K," *Int. J. Metrol. Qual. Eng.* **9**, 13 (2018).
- S. P. Benz and C. A. Hamilton, "A pulse-driven programmable Josephson voltage standard," *Appl. Phys. Lett.* **68**, 3171–3173 (1996).
- N. E. Flowers-Jacobs, A. Rüfenacht, A. E. Fox, P. D. Dresselhaus, and S. P. Benz, "2 Volt pulse-driven Josephson arbitrary waveform synthesizer," in *2016 Conference on Precision Electromagnetic Measurements (CPEM 2016)*, (IEEE, 2016), pp. 1–2.
- R. Schreier, G. C. Temes *et al.*, *Understanding Delta-Sigma Data Converters* (IEEE Press Piscataway, NJ, 2005), Vol. 74.
- P. F. Hopkins, J. A. Brevik, M. Castellanos-Beltran, C. A. Donnelly, N. E. Flowers-Jacobs, A. E. Fox, D. Olaya, P. D. Dresselhaus, and S. P. Benz, "RF waveform synthesizers with quantum-based voltage accuracy for communications metrology," *IEEE Trans. Appl. Supercond.* **29**, 1–5 (2019).
- A. J. Sirois, M. Castellanos-Beltran, A. E. Fox, S. P. Benz, and P. F. Hopkins, "Josephson microwave sources applied to quantum information systems," *IEEE Trans. Quantum Eng.* **1**, 1–7 (2020).
- M. A. Castellanos-Beltran, D. I. Olaya, A. J. Sirois, C. A. Donnelly, P. D. Dresselhaus, S. P. Benz, and P. F. Hopkins, "Single-flux-quantum multiplier circuits for synthesizing gigahertz waveforms with quantum-based accuracy," *IEEE Trans. Appl. Supercond.* **31**, 1–9 (2021).
- J. F. Buzacchelli, L. Hae-Seung, S. Alexandrou, J. A. Misewich, and M. B. Ketchen, "Optoelectronic clocking system for testing RSFQ circuits up to 20 GHz," *IEEE Trans. Appl. Supercond.* **7**, 3301–3306 (1997).
- C. Urano, N. Kaneko, M. Maezawa, T. Itatani, and S. Kiryu, "Pulse driven Josephson voltage standard using modulated optical comb," *J. Phys.: Conf. Ser.* **97**, 012269 (2008).
- J. Nissilä, T. Fordell, K. Kohopää, E. Mykkänen, P. Immonen, R. N. Jabdaraghi, E. Bardalen, O. Kieler, B. Karlsen, P. A. Ohlckers, R. Behr, A. J. Manninen, J. Govenius, and A. Kemppinen, "Driving a low critical current Josephson junction array with a mode-locked laser," *Appl. Phys. Lett.* **119**, 032601 (2021).
- A. M. Weiner, "Ultrafast optical pulse shaping: A tutorial review," *Opt. Commun.* **284**, 3669–3692 (2011).
- A. Monmayrant, S. Weber, and B. Chatel, "A newcomer's guide to ultrashort pulse shaping and characterization," *J. Phys. B: At., Mol. Opt. Phys.* **43**, 103001 (2010).
- C. Huang, Z. Jiang, D. Leaird, J. Caraquiten, and A. Weiner, "Spectral line-by-line shaping for optical and microwave arbitrary waveform generations," *Laser Photonics Rev.* **2**, 227–248 (2008).
- J. T. Willits, A. M. Weiner, and S. T. Cundiff, "Line-by-line pulse shaping with spectral resolution below 890 MHz," *Opt. Express* **20**, 3110–3117 (2012).

- <sup>27</sup>S. T. Cundiff and A. M. Weiner, "Optical arbitrary waveform generation," *Nat. Photonics* **4**, 760–766 (2010).
- <sup>28</sup>A. J. Metcalf, V. Supradeepa, D. E. Leaird, and A. M. Weiner, "Fully programmable two-dimensional pulse shaper for broadband line-by-line amplitude and phase control," *Opt. Express* **21**, 28029–28039 (2013).
- <sup>29</sup>V. R. Supradeepa, C.-B. Huang, D. E. Leaird, and A. M. Weiner, "Femtosecond pulse shaping in two dimensions: Towards higher complexity optical waveforms," *Opt. Express* **16**, 11878 (2008).
- <sup>30</sup>M. Shirasaki, "Large angular dispersion by a virtually imaged phased array and its application to a wavelength demultiplexer," *Opt. Lett.* **21**, 366–368 (1996).
- <sup>31</sup>E. Zielinski, H. Schweizer, K. Streubel, H. Eisele, and G. Weimann, "Excitonic transitions and exciton damping processes in InGaAs/InP," *J. Appl. Phys.* **59**, 2196–2204 (1986).
- <sup>32</sup>S. A. Diddams, L. Hollberg, and V. Mbele, "Molecular fingerprinting with the resolved modes of a femtosecond laser frequency comb," *Nature* **445**, 627–630 (2007).
- <sup>33</sup>L. Nugent-Glandorf, T. Neely, F. Adler, A. J. Fleisher, K. C. Cossel, B. Bjork, T. Dinneen, J. Ye, and S. A. Diddams, "Mid-infrared virtually imaged phased array spectrometer for rapid and broadband trace gas detection," *Opt. Lett.* **37**, 3285–3287 (2012).
- <sup>34</sup>X. Zhu, D. Lin, Z. Hao, L. Wang, and J. He, "A VIPA spectrograph with ultra-high resolution and wavelength calibration for astronomical applications," *Astron. J.* **160**, 135 (2020).
- <sup>35</sup>V. Supradeepa, E. Hamidi, D. E. Leaird, and A. M. Weiner, "New aspects of temporal dispersion in high-resolution Fourier pulse shaping: A quantitative description with virtually imaged phased array pulse shapers," *J. Opt. Soc. Am. B* **27**, 1833–1844 (2010).
- <sup>36</sup>E. Frumker and Y. Silberberg, "Femtosecond pulse shaping using a two-dimensional liquid-crystal spatial light modulator," *Opt. Lett.* **32**, 1384–1386 (2007).
- <sup>37</sup>J. C. Vaughan, T. Hornung, T. Feurer, and K. A. Nelson, "Diffraction-based femtosecond pulse shaping with a two-dimensional spatial light modulator," *Opt. Lett.* **30**, 323–325 (2005).
- <sup>38</sup>S. Xiao and A. M. Weiner, "An eight-channel hyperfine wavelength demultiplexer using a virtually imaged phased-array (VIPA)," *IEEE Photonics Technol. Lett.* **17**, 372–374 (2005).
- <sup>39</sup>G. Kowzan, D. Charczun, A. Cygan, R. S. Trawiński, D. Lisak, and P. Masłowski, "Broadband optical cavity mode measurements at Hz-level precision with a comb-based VIPA spectrometer," *Sci. Rep.* **9**, 8206 (2019).
- <sup>40</sup>I. Coddington, N. Newbury, and W. Swann, "Dual-comb spectroscopy," *Optica* **3**, 414–426 (2016).
- <sup>41</sup>F. Ferdous, D. E. Leaird, C.-B. Huang, and A. M. Weiner, "Dual-comb electric-field cross-correlation technique for optical arbitrary waveform characterization," *Opt. Lett.* **34**, 3875–3877 (2009).
- <sup>42</sup>V. Durán, S. Tainta, and V. Torres-Company, "Ultrafast electrooptic dual-comb interferometry," *Opt. Express* **23**, 30557–30569 (2015).
- <sup>43</sup>Z. Jiang, C.-B. Huang, D. E. Leaird, and A. M. Weiner, "Optical arbitrary waveform processing of more than 100 spectral comb lines," *Nat. Photonics* **1**, 463–467 (2007).
- <sup>44</sup>T. Baumert, T. Brixner, V. Seyfried, M. Strehle, and G. Gerber, "Femtosecond pulse shaping by an evolutionary algorithm with feedback," *Appl. Phys. B: Lasers Opt.* **65**, 779–782 (1997).
- <sup>45</sup>T. Brixner, A. Oehrelein, M. Strehle, and G. Gerber, "Feedback-controlled femtosecond pulse shaping," *Appl. Phys. B* **70**, S119–S124 (2000).
- <sup>46</sup>J. Chou, Y. Han, and B. Jalali, "Adaptive RF-photonic arbitrary waveform generator," *IEEE Photonics Technol. Lett.* **15**, 581–583 (2003).
- <sup>47</sup>K. Ohno, T. Tanabe, and F. Kannari, "Adaptive pulse shaping of phase and amplitude of an amplified femtosecond pulse laser by direct reference to frequency-resolved optical gating traces," *J. Opt. Soc. Am. B* **19**, 2781–2790 (2002).
- <sup>48</sup>H. Ito, T. Nagatsuma, and T. Ishibashi, "Uni-traveling-carrier photodiodes for high-speed detection and broadband sensing," *Proc. SPIE* **6479**, 64790X (2007).
- <sup>49</sup>D. Olaya, P. D. Dresselhaus, and S. P. Benz, "300 GHz operation of divider circuits using high- $J_c$  Nb/Nb<sub>x</sub>Si<sub>1-x</sub>/Nb Josephson junctions," *IEEE Transactions on Applied Superconductivity* **25**, 1–5 (2015).
- <sup>50</sup>Y. Peng, K. Sun, Y. Shen, A. Beling, and J. C. Campbell, "High-power and high-linearity photodiodes at 1064 nm," *J. Lightwave Technol.* **38**, 4850–4856 (2020).
- <sup>51</sup>A. A. Babenko, N. E. Flowers-Jacobs, G. Lasser, J. A. Brevik, A. E. Fox, P. D. Dresselhaus, Z. Popović, and S. P. Benz, "A microwave quantum-defined millivolt source," *IEEE Trans. Microwave Theory Tech.* **69**, 5404–5416 (2021).
- <sup>52</sup>T. Van Duzer and C. W. Turner, *Principles of Superconductive Devices and Circuits* (IEEE, 1981).
- <sup>53</sup>A. Beling, X. Xie, and J. C. Campbell, "High-power, high-linearity photodiodes," *Optica* **3**, 328–338 (2016).